



# Sea ice variability and links to East Siberian permafrost carbon remobilization during the last glacial-interglacial transition

Albin Eriksson<sup>1,2</sup>, Junjie Wu<sup>1,2</sup>, Matt O'Regan<sup>2,3</sup>, and Örjan Gustafsson<sup>1,2</sup>

<sup>1</sup>Department of Environmental Science, Stockholm University, Stockholm, 11418, Sweden.

5 <sup>2</sup>Bolin Centre for Climate Research, Stockholm University, Stockholm, 10691, Sweden.

<sup>3</sup>Department of Geological Sciences, Stockholm University, Stockholm, 10691, Sweden.

*Correspondence to:* Albin Eriksson ([albin.eriksson@aces.su.se](mailto:albin.eriksson@aces.su.se)) and Örjan Gustafsson ([orjan.gustafsson@aces.su.se](mailto:orjan.gustafsson@aces.su.se))

**Abstract.** Sea ice in plays a central role in the polar climate system. In recent decades, the rapid decline of Arctic sea ice has triggered cascading effects the albedo effect and gas/heat transfer in polar regions. Investigations of earlier warming events, such as the Preboreal/Early Holocene (PB/EH, 11-8 kyr B.P), Bølling-Allerød (B/A, 14.7-12.9 kyr B.P), and Dansgaard Oeschger event 3 (DO-3, 28-27.5 kyr B.P), likely hold clues on climate system responses to changes in Arctic sea ice. This study explores the history of sea ice over the Southern Lomonosov Ridge and its potential relation to permafrost carbon remobilization. Sea ice conditions over the last 27 kyrs were reconstructed through a combination of the sea ice biomarker IP<sub>25</sub> (Ice-proxy 25) and marine phytoplankton biomarkers (brassicasterol and dinosterol) from the chronologically well-constrained core 31-PC, sampled at the Southern Lomonosov Ridge during the SWERUS-C3 expedition in 2014. The reconstruction allowed for a direct comparison with previously published terrestrial organic carbon (terrOC) remobilization history from the same core. Our findings revealed a seasonal sea ice cover between 27-26 kyr B.P after the DO-3 warm event, which likely caused more heat and moisture transport from ocean to land and strengthened permafrost thawing along the nearby coastline. A perennial sea ice cover then developed and persisted throughout the Last Glacial Maximum (LGM) to the Younger Dryas (YD), including over the entire B/A warm period. Due to sea-level rise during Meltwater Pulse 1A (MWP 1A, 14.7-13.5 kyr B.P), terrOC remobilization during B/A was rapid but its magnitude smaller when compared to PB and DO-3 in 31-PC, and other records from the Arctic. These records collectively suggest that sea-level rise, rather than sea ice conditions, exerts the primary control on coastal erosion during B/A, while we propose that the perennial sea ice cover may have limited wave-induced coastal erosion on the continental shelf bordering the southern Lomonosov Ridge. A sharp reduction and breakup of the perennial sea ice was observed from the PB to the Early Holocene. Contrary to the B/A, Meltwater Pulse 1B during PB triggered significant coastal erosion and massive terrOC remobilization concurrent with the sea ice decline. The absence of sea ice in parallel to larger coastal erosion compared to B/A implies the role of waning sea ice in enhancing permafrost carbon mobilization along the coastline in this period. In accordance with sea ice records from other Arctic seas, the Holocene record exhibited a period of gradual sea ice expansion. Taken together, these findings highlight sea ice extent as a possible factor regulating coastal permafrost carbon remobilization during the last deglaciation.



## 1 Introduction

Sea ice in polar regions engages in the global climate system through albedo effects and the regulation of heat/gas exchange between the ocean and atmosphere (Solomon 2006; Taylor et al., 2013; Duan et al., 2019). Additionally, sea ice can influence the Atlantic Meridional Overturning Circulation (AMOC) by contributing with meltwaters and regulating exposure of ocean water to sunlight (Sévellec et al., 2017). Thereby, it can affect both regional and even global climate processes. Recently, another coupling between sea ice extent and Arctic climate systems has been suggested. Observations and model simulations suggest that declining sea ice extent can lead to increased wave-induced coastal erosion due to a longer fetch and more frequent open water conditions (Overeem et al., 2011; Barnhart et al., 2014; Nielsen et al., 2020; Nielsen et al., 2024). Paleoclimate evidence implies that this could have been important in past periods of abrupt climate change with reduced sea ice conditions enhancing permafrost thawing and subsequent greenhouse gas releases (Vaks et al., 2020). Taken together, Arctic sea ice exerts significant control over key processes in the current and past climate, underscoring the need for further assessments of the role of sea ice in affecting climate-related processes.

Fundamentally, anthropogenic activities and associated greenhouse gas emissions are the main triggers for recent Arctic warming and sea ice retreat. However, the Arctic sea ice history beyond instrumental records can provide further clues on system functioning, including past effects and causes of Arctic climate change. Current paleoclimate evidence for Arctic sea ice is usually temporally limited to the Holocene or does not cover the full deglaciation process from the Last Glacial Maximum (LGM), particularly in the East Siberian Arctic (e.g. Fahl & Stein 2012; Xiao et al., 2015; Hörner et al., 2016; Stein et al., 2017; Lin et al., 2024). Consequently, the role of sea ice in the global climate during periods of abrupt climate change requires further investigation. Specific molecular biomarkers of ice-associated phytoplankton, the highly branched isoprenoid alkenes (HBI) can be used as proxies to trace sea ice in the past (Belt et al., 2007). A commonly used HBI for sea ice reconstructions is IP<sub>25</sub> (ice-proxy 25). However, the application of IP<sub>25</sub> is limited by two scenarios when IP<sub>25</sub> is absent, ice-free and permanent sea ice conditions (Belt et al., 2018). To address this issue, the PIP<sub>25</sub> index (phytoplankton-IP<sub>25</sub>) was introduced, where phytoplankton biomarkers such as brassicasterol and dinosterol indicate whether the absence of IP<sub>25</sub> is caused by ice-free or permanent sea ice conditions (e.g., Müller et al., 2011; Xiao et al., 2013; Xiao et al., 2015; Stein et al., 2017). Applications of the PIP<sub>25</sub> index can provide a more comprehensive understanding of sea ice-climate interactions in the East Siberian Arctic during the last deglaciation.

The East Siberian Arctic holds extensive quantities of organic carbon (OC) within permafrost. The destabilization of this permafrost has historically, and continues to contribute to the significant remobilization of OC into the Arctic Ocean (e.g., Vonk et al., 2012; Köhler et al., 2014; Tesi et al., 2016; Martens et al., 2020, 2022; Wu et al., 2025; Vonk et al., 2025). The key mechanisms driving permafrost OC remobilization during the last deglaciation primarily include coastal erosion of the East Siberian Arctic Shelf due to sea level rise, active layer thawing, and subsequent riverine transport of OC (Tesi et al., 2016;



65 Martens et al., 2020; Lin et al., 2025; Nicolas et al., 2025). Given the substantial OC reservoirs in Arctic permafrost and their potential impact on climate change, the understudied influence of sea ice dynamics on wave-induced coastal erosion warrants further investigation to better define terrestrial OC (terrOC) remobilization processes.

Permafrost carbon exhibits distinct isotopic characteristics depending on its formation time, which provide valuable clues for  
70 constraining carbon sources and their remobilization mechanisms. Ice Complex Deposits (ICD), also known as Yedoma, formed during the Pleistocene and are characterized by huge ice wedges and old radiocarbon ages, and are usually remobilized through thaw-induced coastal erosion (Vonk et al., 2012; Strauss et al., 2017). On the other hand, surficial permafrost consists of comparatively young radiocarbon and can be remobilized through processes such as active layer thawing and riverine erosion (Martens et al., 2020, 2022; Matsubara et al., 2022; Wu et al 2025). By deconvoluting the source fingerprint of OC  
75 accumulating in the receptor sediments, it is possible to identify sources and mechanisms of permafrost carbon remobilization. Specifically, the source contribution can be investigated by analysing stable carbon isotopes ( $\delta^{13}\text{C}$ ) to differentiate between marine and terrestrial OC (Semiletov et al., 2005; Martens et al., 2021). The relative contribution within the terrOC pool (such as surficial permafrost and erosion of deeper permafrost layers) can be further resolved by combining  $\delta^{13}\text{C}$  with radiocarbon dating ( $^{14}\text{C}$ ) given the age difference of the OC in these different permafrost pools (Gustafsson et al. 2011; Vonk et al., 2012;  
80 Karlsson et al., 2016; Wild et al., 2019; Martens et al., 2022). To further investigate mechanisms of remobilization, terrigenous biomarkers (sterols, lignin etc) can trace the input of terrestrial OC (terrOC) and provide further information about the origin of OC (Kremer et al., 2018; Tesi et al., 2016; Bröder et al., 2018; Matsubara et al., 2022). In summary, the carbon isotopic characteristics combined with terrigenous biomarkers enables source tracing of the sedimentary OC input, and the potential mobilization mechanisms.

85

In this study, we aim to investigate the sea ice history around the Southern Lomonosov Ridge to better understand sea ice changes during periods of abrupt climate change and their impacts on the remobilization of terrOC along permafrost coastlines. We utilized the well-characterized sediment core 31-PC from the Southern Lomonosov Ridge, located off the Laptev and East Siberian Seas (Fig. 1; Muschitiello et al., 2020; Martens et al., 2020). By reconstructing the sea ice history over the last 27  
90 kyrs using  $\text{IP}_{25}$  and the  $\text{PIP}_{25}$  index, we provide a detailed temporal record. Additionally, we incorporate findings from a isotope-based carbon source apportionment study on the same core (Martens et al., 2020) to explore the connection between sea ice and permafrost carbon remobilization.

## 2 Methods

### 2.1 Material and study area

95 During the SWERUS-C3 expedition in 2014 on the Swedish icebreaker *Oden*, an eight-meter-long piston core (31-PC) was obtained at 1120 m depth on the Southern Lomonosov Ridge (79.91°N, 143.23°E, Fig. 1). Due to disturbance of the surface



sediments during the piston coring processes, surface sediment, representing the top of the core was used from multicore 31-MUC, sampled at the same location. The chronology of core 31-PC was established through a combination of radiocarbon dating and stratigraphic correlation with ice-core records from Greenland, encompassing the last 27 kyr (Muschitiello et al., 2020; Martens et al., 2020). The age-model is described in detail in Muschitiello et al. (2020). The sampling location on the intersection between the Siberian continental margin and the Southern Lomonosov Ridge enabled sea ice reconstructions encompassing parts of the East Siberian- and Laptev Sea. Additionally, the sampling location enabled quantification of fluviually transported inland PF-C from the Lena River throughout the last deglaciation, including the Holocene. Notably, the core site was adjacent to ICD PF on the continental shelf, which formed during low sea levels and exposed deposits that are now submerged as subsea permafrost. This makes the core site an important receptor for terrOC from past shelf flooding and coastal erosion.

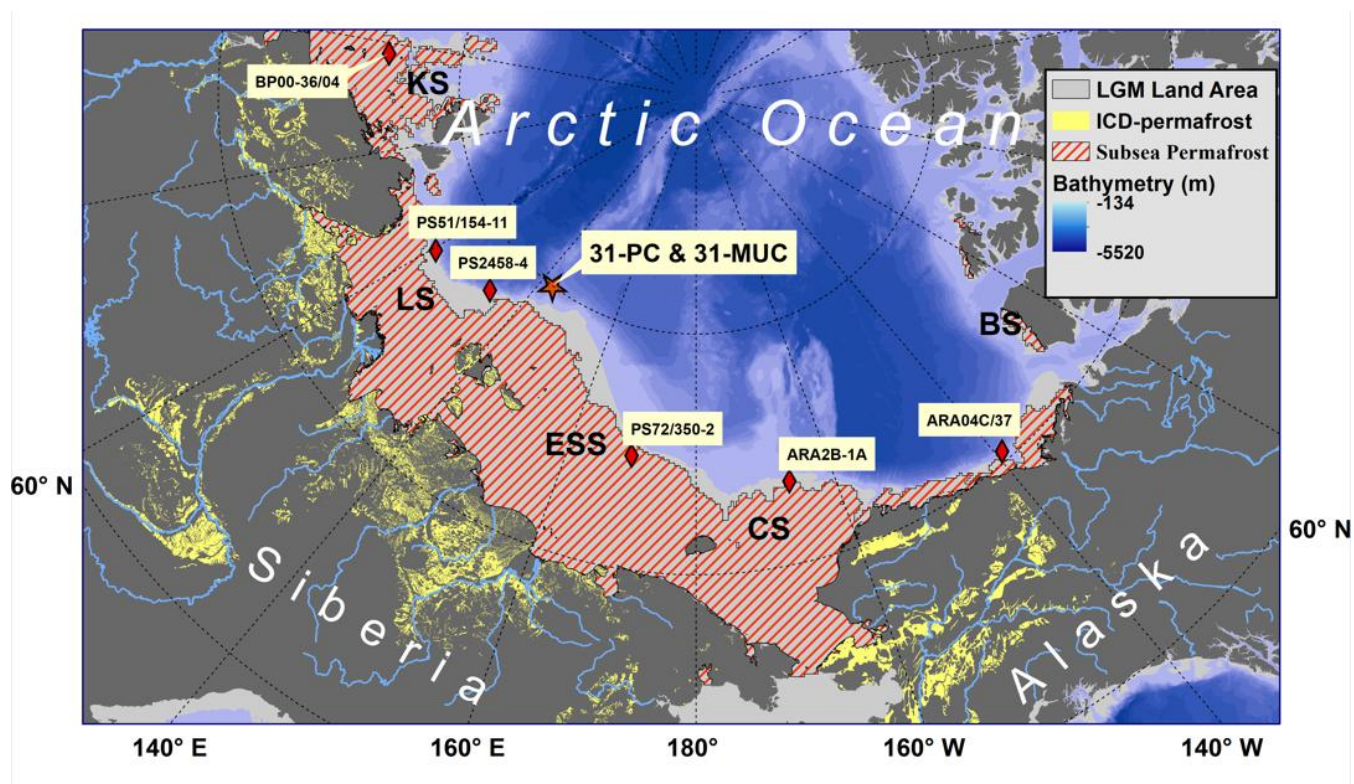


**Figure 1:** Sampling location of 31-PC and 31-MUC are indicated with a star marker. Other paleorecords of sea ice reconstruction discussed in this study are indicated with red rhombic markers. The current shelf seas of the Kara Sea (KS), Laptev Sea (LS), the East Siberian Sea (ESS), Chukchi Sea (CS), and Beaufort Sea (BS) are clarified with abbreviations. Bathymetry was applied using IBCAO version 4.2 (Jakobsson et al., 2022). The light-gray areas indicate land during the last glacial maximum (LGM), which were flooded during the last deglaciation. Yellow areas are contemporary land regions covered by ICD-permafrost (Strauss et al., 2022), and red lines display subsea permafrost in the contemporary Arctic (Overduin et al., 2019). Contemporary Arctic rivers are displayed as light blue lines.



## 2.2 Lipid Biomarkers

115 The biomarker analyses were carried out following the method initiated by Belt et al. (2012), with minor modifications. Briefly, freeze-dried sediment samples were homogenised and ground to fine powders, followed by additions of 20  $\mu\text{l}$  of 7-hexylnonadecane ( $0.00465 \mu\text{g } \mu\text{l}^{-1}$ ), 9-octylheptadec-8-ene ( $0.00535 \mu\text{g } \mu\text{l}^{-1}$ ), and androstanol ( $0.45 \mu\text{g } \mu\text{l}^{-1}$ ), respectively, as internal standards to correct for analyte losses during the laboratory procedure. Lipid extraction was performed on the sediments with saponification using KOH (5%, MeOH/H<sub>2</sub>O: 9/1, v/v; KOH  $\geq$  85% purity; MeOH  $\geq$  99,9% purity), heating for 120 1h at 70 °C. The saponified contents were then extracted by repeated liquid-liquid extractions with hexane after vortexing and centrifugating the samples. Condensed extracts were eluted into a non-polar (using 6 ml *n*-hexane) and a polar fraction (using 6 ml DCM/MeOH, 1:1, v/v) through open-column chromatography with 1 % H<sub>2</sub>O deactivated silica gel (63-200  $\mu\text{m}$ ; Supelco) as the stationary phase.

125 Before instrumental analyses, the polar fraction was derivatized with N, O-Bis (trimethylsilyl) trifluoroacetamide (BSTFA) at 70°C for 1h. Both polar and non-polar fractions were analysed using gas chromatography-mass spectrometry (GC-MS) (GC-MS 7820-A, Agilent Technologies USA). Non-polar compounds were analysed in splitless mode using single ion monitoring mode (SIM), starting at a temperature of 40°C, ramping up 10°C per minute up to a maximum temperature of 300°C for 10 minutes. To minimize potential carryover, a one-minute post-run at 305°C was conducted for each sample. The polar fraction 130 was analysed in splitless mode using total ion current mode (TIC), with a starting temperature of 60°C held for one minute, followed by a 10°C per minute temperature ramp to a maximum temperature of 310°C, maintained for 16 minutes.

Identification of IP<sub>25</sub> was based on the retention times of the compound in reference sediments provided by Professor Simon Belt (University of Plymouth). The target sterol compounds were identified based on the mass fragmentation pattern, and 135 monitored through selective ion chromatograms, *m/z* 348, 470, 472, 486, 500 (androstanol, brassicasterol, campesterol,  $\beta$ -sitosterol, and dinosterol). Quantifications of both fractions were based on the differences in mass spectral responses of the target compounds and the internal standards, following the method of Belt et al., (2012). Additionally, the PIP<sub>25</sub>-indices (Eqs. 1 & 2) were calculated according to Müller et al., (2011).

$$PIP_{25} = \frac{[IP_{25}]}{[IP_{25}] + ([P] * c)} \quad (1)$$

140

$$c = \frac{\text{mean } [IP_{25}]}{\text{mean } [P]} \quad (2)$$

Where P is a phytoplankton biomarker (e.g., brassicasterol or dinosterol), and c is the concentration balance factor to account for concentration differences in IP<sub>25</sub> and phytoplankton biomarkers (Müller et al., 2011).



## 2.3 Carbon characteristics

The stable carbon isotope ratio ( $\delta^{13}\text{C}$ ) and radiocarbon ( $\Delta^{14}\text{C}$ ) content in the surface sediment of 31-MUC was analysed through  
145 accelerator mass spectrometry at the Tandem Laboratory, Uppsala University. The other carbon isotopic composition and  
radiocarbon ages of OC in 31-PC were already published and re-used from Martens et al. (2020). However, new pre-  
depositional ages of the OC were employed in this study, now with the ages further corrected for atmospheric  $\Delta^{14}\text{C}$  changes,  
according to Intcal20 (Reimer et al., 2020). The radiocarbon at the time of deposition ( $\Delta^{14}\text{C}_{\text{initial}}$ ) was calculated through Eq.  
(3) (Scheffuß et al. 2016).

$$150 \quad \Delta^{14}\text{C}_{\text{initial}} = (F^{14}\text{C}e^{\lambda t} - 1) * 1000\text{‰} \quad (3)$$

Where  $F^{14}\text{C}$  is the fraction modern carbon,  $t$  is the time of deposition, and  $\lambda$  the decay constant for radiocarbon. Furthermore,  
the pre-depositional age (years) was subsequently corrected through Eq. (4) (Scheffuß et al. 2016).

$$\text{Pre - depositional age} = -8033 * \ln \left[ \frac{1 + \frac{\Delta^{14}\text{C}_{\text{initial}}}{1000}}{1 + \frac{\Delta^{14}\text{C}_{\text{atm}}}{1000}} \right] \quad (4)$$

## 3 Results

155 In the core-bottom ~27 kyr B.P., high concentrations and fluxes of marine and terrestrial biomarkers were observed. After the  
DO-3 (28-27.5 kyr B.P, Dansgaard et al., 1993) around ~26.6-27 kyr B.P., core 31-PC the concentrations of  $\text{IP}_{25}$  (0.20-0.36  
 $\mu\text{g gOC}^{-1}$ ), dinosterol (7.60-24.8  $\mu\text{g gOC}^{-1}$ ), and brassicasterol were relatively elevated (23.5-30.6  $\mu\text{g gOC}^{-1}$ ; Fig. 2 & 3).  
Concurrently, massive fluxes of dinosterol (52.2-170.9  $\mu\text{g m}^{-2} \text{yr}^{-1}$ ) and brassicasterol (179.4-270.6  $\mu\text{g m}^{-2} \text{yr}^{-1}$ ; Fig. 3) were  
present. The  $\text{PIP}_{25}$  indices during this period ranged from approximately 0.2-0.4 (Fig. 3). Moreover, the aftermath of DO-3  
160 was marked by high fluxes and concentrations of campesterol (181.5-269.5  $\mu\text{g m}^{-2} \text{yr}^{-1}$ ; 25.2-43.7  $\mu\text{g gOC}^{-1}$ ) and  $\beta$ -sitosterol  
(462.6-579.8  $\mu\text{g m}^{-2} \text{yr}^{-1}$ ; 66.7-84.5  $\mu\text{g gOC}^{-1}$ ). Around 26.5 kyr B.P., the fluxes and concentrations of these biomarkers  
diminished toward the LGM, with a concurrent abrupt increase in  $\text{PIP}_{25}$  (Fig. 3, 4 & 5).

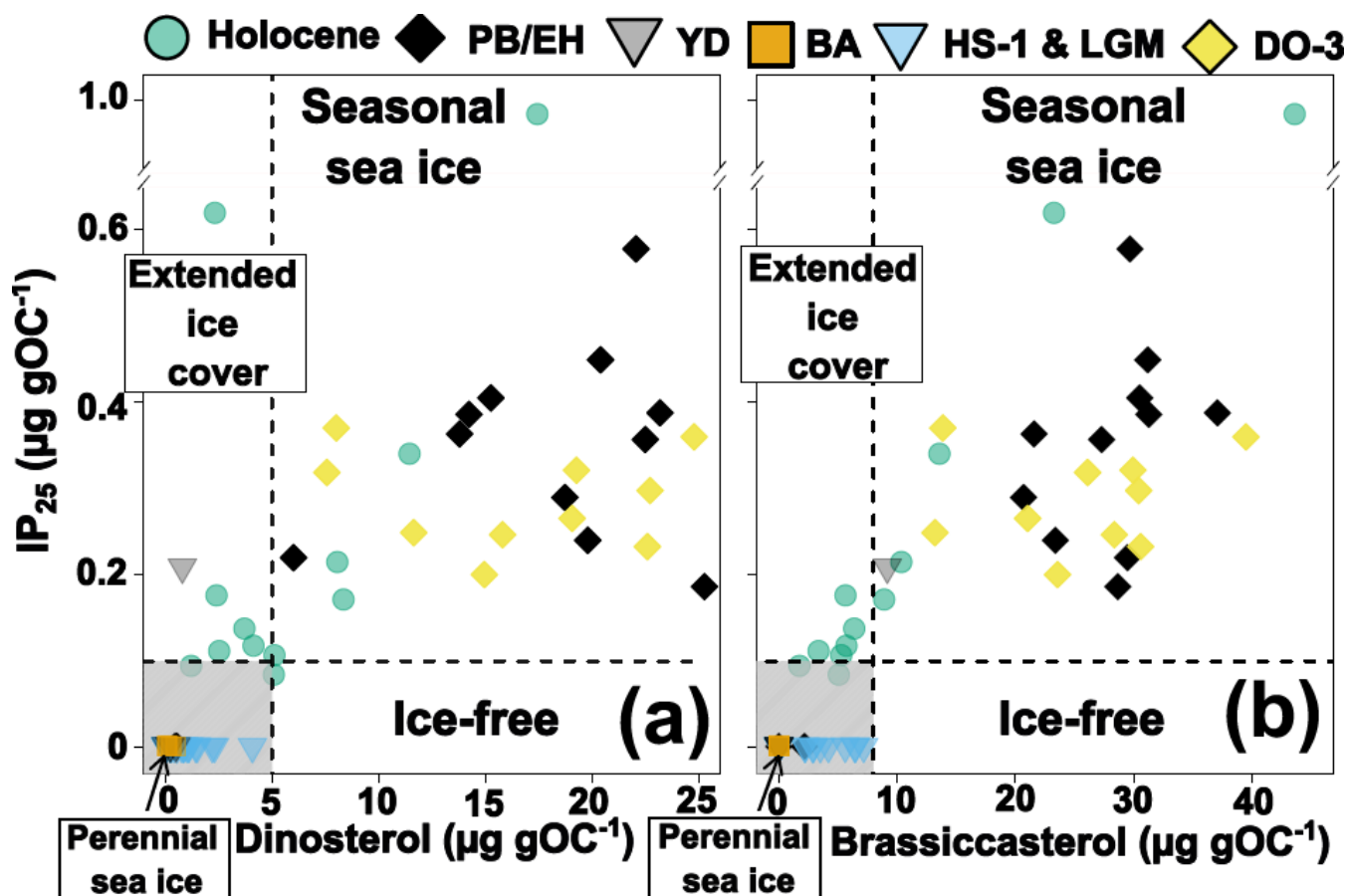
From the LGM to around 11 kyr BP,  $\text{IP}_{25}$ , dinosterol and brassicasterol declined to non-detectable levels, with only occasional  
165 low concentrations of dinosterol and brassicasterol (Fig. 2 & 3). Consequently, no  $\text{PIP}_{25}$  indices are reported for this period  
(Fig. 3). Similarly, the fluxes and concentrations of campesterol and  $\beta$ -sitosterol remained relatively low from the LGM until  
11 kyr BP, with only minor increases noted around ~17-21 kyr B.P, and during B/A (Fig.3).

Following a long period of non-detectable  $\text{IP}_{25}$  and extremely low concentrations of marine biomarkers extending between  
170 ~26-11 kyr B.P., the biomarker input abruptly shifted. In the PreBoreal and early Holocene (PB/EH) the highest concentrations  
of  $\text{IP}_{25}$  (0.19-0.39  $\mu\text{g gOC}^{-1}$ ), dinosterol (6.0-25.3  $\mu\text{g gOC}^{-1}$ ) and brassicasterol (20.7-37.0  $\mu\text{g gOC}^{-1}$ ) were observed (Fig. 2 &  
3). The  $\text{PIP}_{25}$  indices during this period fluctuated between approximately 0.14 and 0.54 (Fig. 3). Moreover, the PB/EH marked



175 elevated fluxes of these phytoplankton tracing biomarkers (Fig. 3). Parallel to the algal biomarker increases, the terrestrial biomarker fluxes and concentrations of campesterol ( $6.86\text{-}338.3 \mu\text{g m}^{-2} \text{yr}^{-1}$ ;  $6.41\text{-}59.7 \mu\text{g gOC}^{-1}$ ) and  $\beta$ -sitosterol ( $61.2\text{-}976.9 \mu\text{g m}^{-2} \text{yr}^{-1}$ ;  $34.2\text{-}172.3 \mu\text{g gOC}^{-1}$ ) were amplified during the PB/EH (Fig. 3).

As the Holocene progressed, the initially high fluxes and concentrations of IP<sub>25</sub>, dinosterol, and brassicasterol gradually diminished, though a notable abrupt increase occurred around ~7-8 kyr B.P., followed by a gradual decline until ~1 kyr B.P. (Fig. 3). Correspondingly, the PIP<sub>25</sub> indices gradually increased towards modern conditions (Fig. 3). In the mid-late Holocene, 180 both campesterol and  $\beta$ -sitosterol exhibited gradual decreases in concentrations and fluxes, with the exception of amplified levels around ~4 kyr B.P. and in the modern core-top sample (~0 kyr B.P.; Fig. 3).



185 **Figure 2:** Sea ice distribution across the 27 kyrs recorded in 31-PC. Yellow diamond markers display the aftermaths of DO-3 (27-27.2 kyr B.P.), orange rectangular markers B/A, and black diamond markers the PB/EH. Inverted triangles show stadial conditions, and green circles indicate the Holocene. Black dashed lines distinguish the different extent of sea ice coverage.

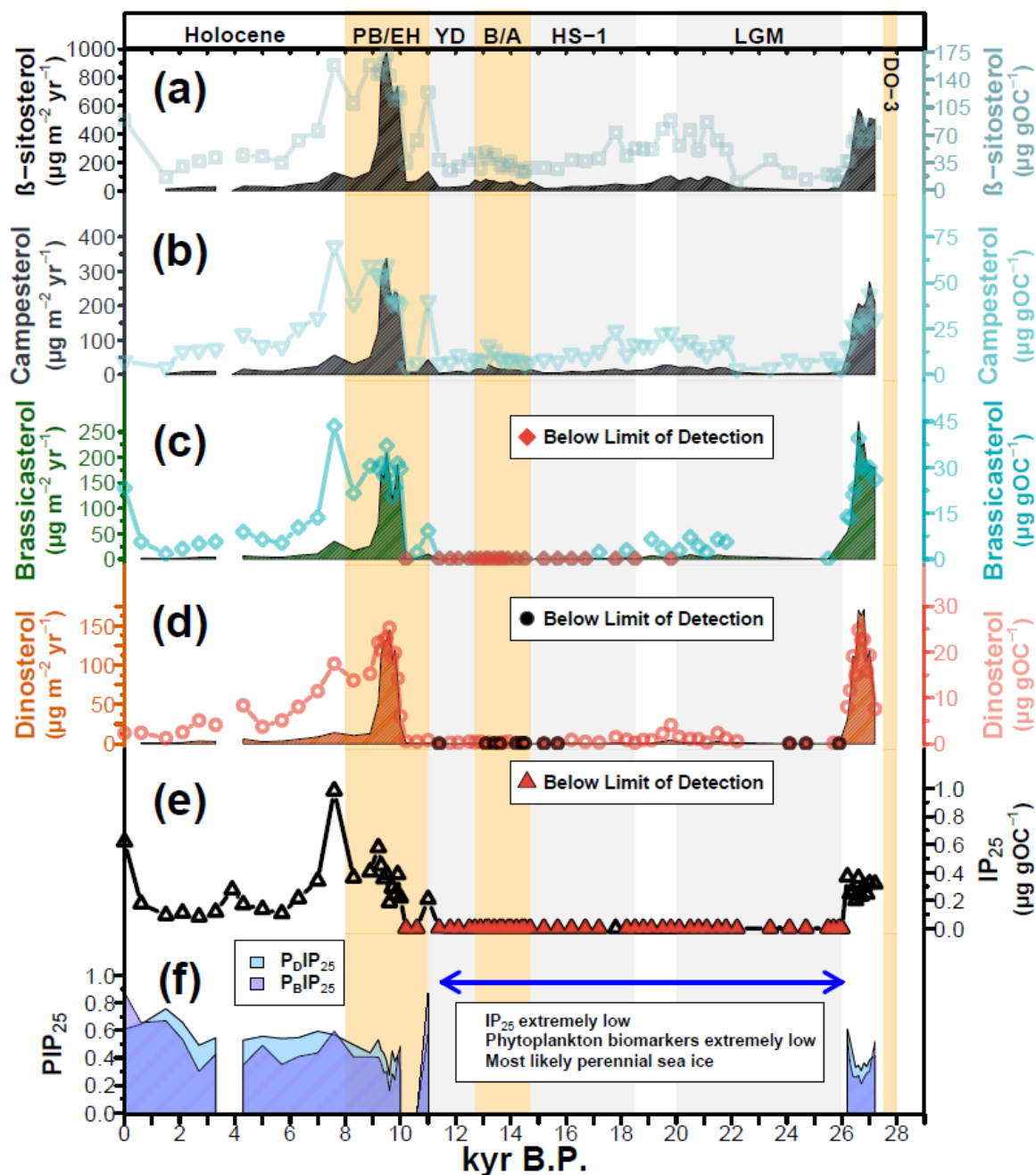


**Figure 3:** Biomarker fluxes and concentrations recorded in 31-PC ( $\mu\text{g m}^{-2} \text{yr}^{-1}$ ;  $\mu\text{g gOC}^{-1}$ ). Red filled markers indicate concentrations below the limit of detection. a)  $\beta$ -sitosterol fluxes (dark brown), and concentrations (light blue-green). b) campesterol fluxes (dark gray) and concentrations (turquoise). c) Brassicasterol fluxes (green), and concentrations (light blue). d) Dinosterol fluxes (orange), and concentrations (light purple). e)  $\text{IP}_{25}$  concentrations (black). f)  $\text{PIP}_{25}$  indices, the darker shade of blue indicates  $\text{P}_{\text{B}}\text{IP}_{25}$ , and the lighter shade  $\text{P}_{\text{D}}\text{IP}_{25}$ . The interval 11-26 kyr B.P., is not displayed due to  $\text{IP}_{25}$  and brassicasterol remaining below the limit of detection or in extremely low concentrations, yielding unreliable  $\text{PIP}_{25}$  indices



## 4 Discussion

### 4.1 Seasonal sea ice and enhanced terrOC transport during the DO-3 interstadial

195 The Dansgaard-Oeschger (DO) events are characterized by rapid increases in atmospheric and sea surface temperatures, along with significant changes in hydrology (Dansgaard et al., 1993; Jensen et al., 2018). The DO-3 event (28-27.5 kyr B.P) is likely recorded in 31-PC (spanning  $27.2 \pm 2.3/-1.4$  kyr B.P; Muschitiello et al., 2020; Fig.3). The relatively low PIP<sub>25</sub> during this time suggest that the DO-3 likely led to approximately ~1 kyr of seasonal sea ice conditions, persisting until the transition into the LGM at 26 kyr B.P. This contrasts with earlier findings from the Southern Lomonosov Ridge (PS2767-4) that reported  
200 increased sea ice preceding the LGM (Xiao et al., 2015). However, this earlier study was based on a low-resolution core using a less well-constrained age model that was subsequently re-interpreted based on the improved dating of 31-PC (Muschitiello et al., 2020). Conclusively attributing seasonal sea ice conditions during/after DO-3 to increased temperatures is still challenging, given that the onset of DO-3 is not captured in this record. Nevertheless, the amplified phytoplankton productivity following DO-3 was likely associated with seasonal sea ice cover and/or marginal ice zones. Nutrient input from melting sea  
205 ice may have contributed to the enhanced IP<sub>25</sub>, dinosterol, and brassicasterol (Fig. 3: Belt et al., 2018), and the increased input of marine OC to the core location (Fig. 5; Martens et al., 2020). As DO-3 progressed into its later stages, the increasing PIP<sub>25</sub> values indicate an expanding sea ice cover approaching the LGM (Fig. 3 & 4).

Succeeding the DO-3, 31-PC recorded an abrupt increase in terrestrial biomarkers, consistent with the high input of OC  
210 observed in core 31-PC (Fig. 4 & 5; Martens et al., 2020). The terrestrial OC is characterized by young pre-depositional ages of ~4-7 kyrs (Fig. 5). Accordingly, previous research attributed the significant input of terrestrial OC to active layer thawing, caused by warming during DO-3 (Martens et al., 2020). However, our records of reduced sea ice may suggest additional mechanisms causing active layer thawing, associated with heat and moisture transport during times of open water conditions. Specifically due to the proximity of the core location to the paleo-shoreline at the time (Fig. 1). The reduced sea ice after DO-  
215 3 may have led to higher air temperatures, which, combined with increased moisture sources, could result in heavy autumn snowfall. This snow could insulate the permafrost from low winter temperatures, leading to further thawing, as was displayed by Vaks et al., (2020). Consequently, the more frequent open water conditions observed in core 31-PC following DO-3, persisting for about 1 kyr or longer, may have contributed to the remobilization of permafrost carbon and observed enhancement of terrestrial OC input. Taken together, core 31-PC represents the first high-resolution record of sea ice history  
220 following DO-3 in this region, providing valuable insights into the impact of sea ice impact on permafrost carbon remobilization.

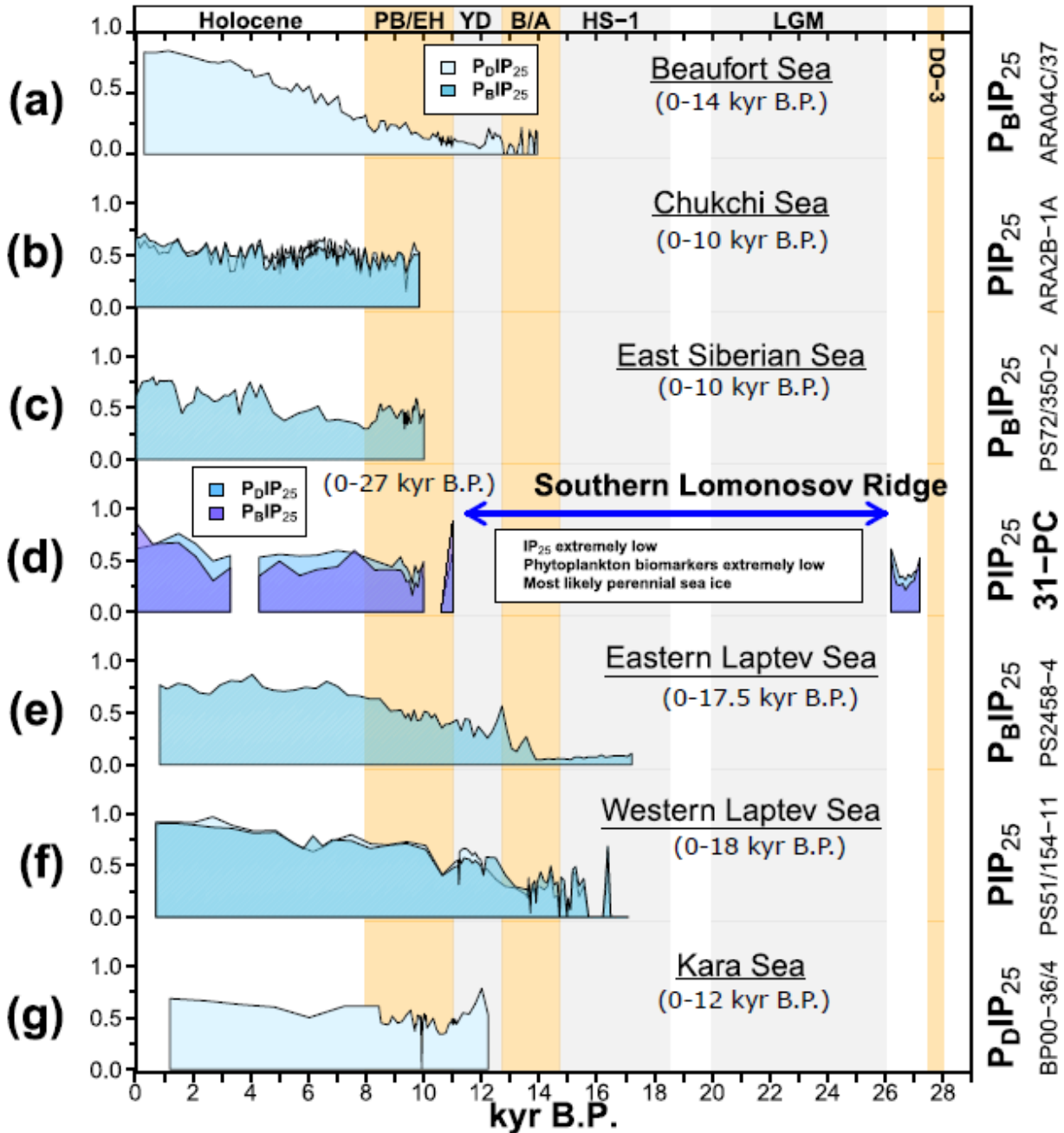


**Figure 4:** Temporal distribution of reconstructed PIP<sub>25</sub> sea ice in marine sediment cores across the Arctic Ocean during the last 27.2 kyr B.P.. a) P<sub>D</sub>IP<sub>25</sub> in a Beaufort Sea sediment core covering the last 14 kyr (Wu et al., 2020). b) Chukchi Sea sediment core covering the last 10 kyr (Stein et al., 2017). c) P<sub>B</sub>IP<sub>25</sub> in an East Siberian Sea sediment core covering the last 10 kyr (Stein et al., 2017). d) The 31-PC record covering the last 27.2 kyr. The interval 11-26 kyr B.P., is not displayed due to IP<sub>25</sub> and brassicasterol remaining below the limit of detection or in extremely low concentrations, yielding unreliable PIP<sub>25</sub> indices (Fig. 3). e) P<sub>B</sub>IP<sub>25</sub> in a nearby core from the Laptev Sea, covering the last 17.5 kyr (Fahl and Stein., 2012). f) Western Laptev Sea sediment core covering the last 18 kyr (Hörner et al., 2016; Lin et al., 2024). g) P<sub>D</sub>IP<sub>25</sub> in a Kara Sea sediment core covering the last 12 kyr (Hörner et al., 2018).

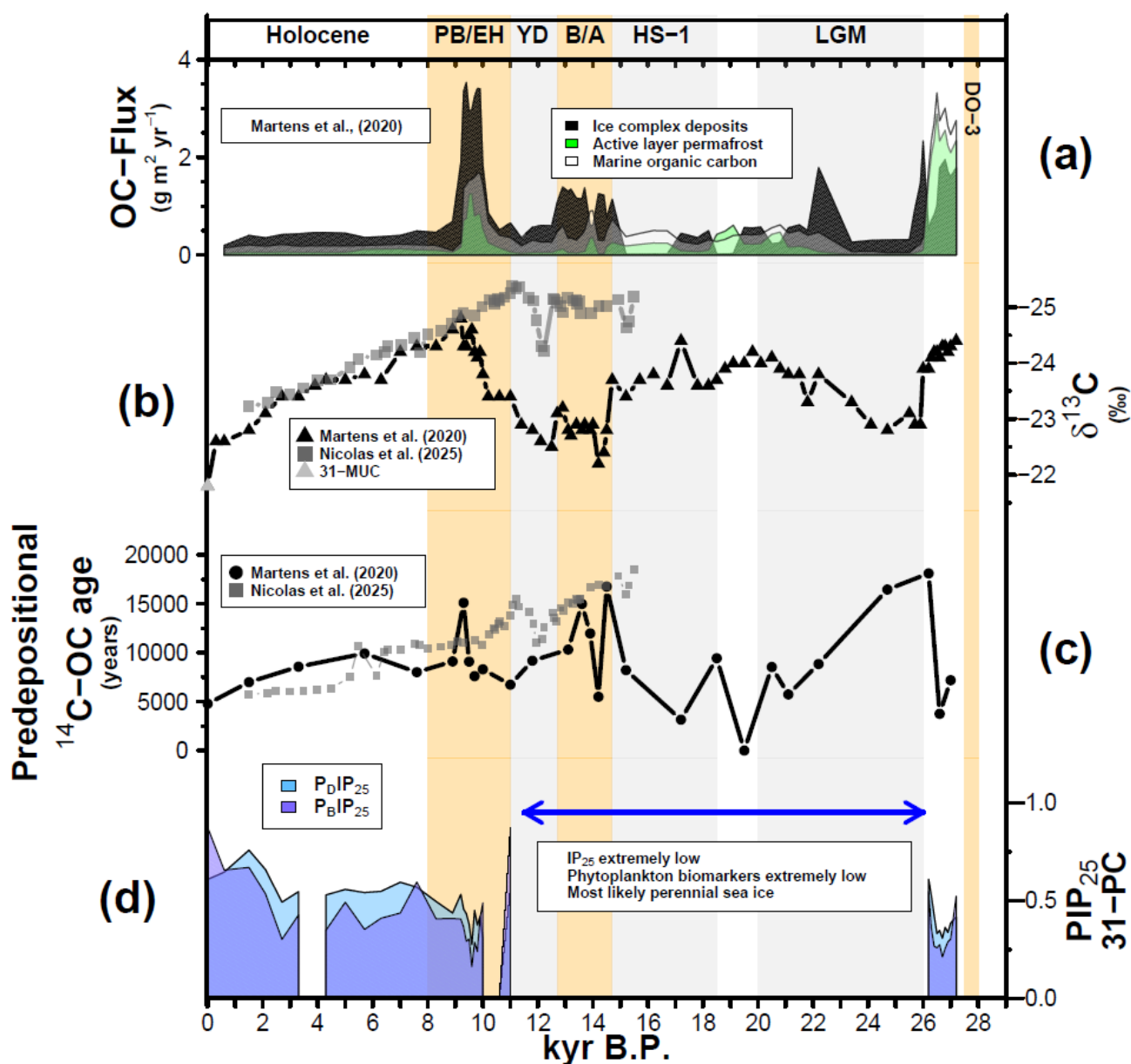
225



#### 230 **4.2 Perennial sea ice and limited terrOC input during the LGM and HS-1 stadial**

During the cold stadial of LGM and HS-1, the concentrations of IP<sub>25</sub> and marine phytoplankton biomarkers were below detection limits (Fig. 3), indicating the presence of permanent sea ice. The absence of these biomarkers suggests that thick sea ice inhibited the growth of open-water phytoplankton by limiting light penetration and hindering ice algae growth. In contrast to studies that artificially set the PIP<sub>25</sub> index to 1 in the absence of both sea ice and marine phytoplankton biomarkers, our records emphasize the absence of these biomarkers to highlight the presence of permanent sea ice (Fig. 3). These results contrast with studies from the Laptev Sea, which suggests the existence of seasonal sea ice or even ice-free conditions during the HS-1 (Hörner et al., 2016; Fahl and Stein, 2012). The different sea ice conditions between the Southern Lomonosov Ridge and the nearby Laptev Sea may be attributed to the influence of warm Atlantic Water (Bradley & England., 2007). It is possible that this warm current has reduced sea ice in the Laptev Sea, while the Southern Lomonosov Ridge and the adjacent East Siberian Sea were less affected by this warm inflow and maintained permanent sea ice (Xiao et al., 2015). This could also explain the near absence of pre-Holocene sediment records in the East Siberian Sea. However, further studies are necessary to validate this hypothesis.

The input of the terrestrial biomarkers campesterol and  $\beta$ -sitosterol was significantly reduced during the LGM and HS-1 (Fig. 3). Previous studies have attributed this decline to the stabilization of permafrost under the cold climate (Martens et al. 2020). Our findings suggest that permanent sea ice could serve as a barrier for transport of terrestrial matter into the marine environment. It is also worth noting that the presence of permanent sea ice likely reduced the fetch distance and wave activity, thereby protecting coastal areas from erosion and minimizing the input of older carbon sources such as those from ICD-PF. During the LGM, the reduction of wave-induced coastal erosion is apparent despite the proximity to the ICD-coastline (Fig.1). Interestingly, our records show a minor increase in terrestrial biomarkers and brassicasterol between ~19-22 kyr B.P., while such an increase was absent in dinosterol (Fig. 3). Given that brassicasterol may have lacustrine sources (Hörner et al., 2016), this increase may indicate a moderate rise in material from riverine input. However, the underlying cause of this increase remains unclear, especially considering the cold climate, presence of permanent sea ice (Fig. 3), and relatively stable sea levels (Lambeck et al., 2014).



255

260

**Figure 5:** Carbon characteristics and PIP<sub>25</sub> reconstructed sea ice using the 31-PC record. a) Organic carbon fluxes ( $\text{g m}^{-2} \text{yr}^{-1}$ ) based on source apportionments from Martens et al., (2020). b) Stable isotopic signature ( $\delta^{13}\text{C-OC}$ ) of 31-PC from Martens et al., (2020), including the addition of the surface layer from 31-MUC ~0 kyr B.P. Stable isotopic signature ( $\delta^{13}\text{C-OC}$ ) of Eastern Laptev Sea core PS2458-4 (Nicolas et al., 2025). c) Recalculated predepositional age of  $^{14}\text{C-OC}$  at the time of atmospheric carbon sequestration in 31-PC (Martens et al., 2020), and predepositional age of  $^{14}\text{C-OC}$  in Eastern Laptev Sea core PS2458 (Nicolas et al., 2025). d) PIP<sub>25</sub> reconstructed sea ice with dinosterol ( $\text{P}_\text{DIP}_{25}$ ) and brassicasterol ( $\text{P}_\text{BIP}_{25}$ ) as the phytoplankton biomarkers. The blue arrow indicates the time when individual phytoplankton and IP<sub>25</sub> were extremely low, yielding unreliable PIP<sub>25</sub>-indices, see Fig.3 for reference.



#### 4.3 Perennial sea ice persisting into the Younger Dryas with limited terrOC input present during the Bølling-Allerød interstadial

265 During the YD stadial, and despite the warming climate of the B/A, the IP<sub>25</sub> and open-water algae biomarkers remained undetectable, comparable to the levels observed during the LGM (Fig. 3). This suggests that permanent sea ice persisted from the LGM until approximately 11 kyr BP. This sea ice condition contrasts with the patterns observed in the Kara Sea, Laptev Sea, and the Beaufort Sea, where sea ice cover was reduced during the B/A and slightly increased during the YD, but generally remained seasonal (Fig. 4; Hörner et al., 2016; Hörner et al., 2018; Fahl and Stein, 2012; Wu et al., 2020). Lin et al. (2024)  
270 proposed that during this time, Atlantic Water inflow inhibited sea ice formation in the Laptev Sea. Similar to the conditions during the LGM and HS-1. Therefore, the persisting sea ice cover in the Southern Lomonosov Ridge and Eastern Laptev Sea is possibly due to the less profound impact of warm Atlantic Water inflow to our study area.

In the context of permanent sea ice, there was a modest increase in terrestrial input during the B/A, coupled with a notable  
275 increase in the pre-depositional age of OC, reaching approximately 15 kyr (Fig. 3&5). This implies the involvement of additional mechanisms that remobilized older permafrost carbon. Typically, permanent sea ice is expected to reduce wave activity, thereby limiting coastal erosion, and to decrease heat and moisture transport, which reduces inland permafrost thawing (Barnhart et al., 2014; Vaks et al., 2020). Thus, the observed increase in permafrost carbon remobilization is likely linked to the shelf flooding induced by sea-level rise during the meltwater pulse 1A (MWP-1A; Lambeck et al., 2014; Martens et al.,  
280 2020). This indicates that permafrost carbon remobilization during the B/A was primarily influenced by sea-level rise rather than by sea ice conditions in our study location. It is important to note that the magnitude of permafrost remobilization recorded in core 31-PC is moderate compared to the DO-3 and PB events, as well as compared to the Sea of Okhotsk, Bering Sea, North Pacific, and Beaufort Sea, where extensive remobilization during the B/A has been widely documented (Winterfeld, et al., 2018; Meyer et al., 2019; Wu et al., 2022). This suggests a significant role of the permanent sea ice limiting coastal erosion  
285 during B/A. Especially considering that nearby cores in the Eastern (PS2458; Fahl and Stein, 2012) and Western Laptev Sea (PS51-154/11; Hörner et al., 2016) display open water/seasonal sea ice conditions concurrent to input of pre-aged OC/*n*-alkanoid acids, but in several orders of magnitude higher fluxes than in 31-PC (Fig. 5; Nicolas et al., 2025). Granted that permanent sea ice likely limited the transport of terrOC to the core site, the actual magnitude of terrOC input driven by sea-level rise in this region remains uncertain and warrants further investigation.

290

During the YD stadial, terrestrial input returned to low levels, comparable to the marine contributions as indicated by the marine phytoplankton biomarkers and carbon source apportionment (Fig. 3; Martens et al., 2020). Overall, the low terrestrial input and young pre-depositional age suggest that the cold climate of the YD likely contributed to the stabilization of permafrost, and the permanent sea ice may have had an additional effect on this stabilization.



#### 295 **4.4 Breakup of perennial sea ice and increased terrOC input during the Early Holocene**

During the transition of PB/EH, there was a marked increase in IP<sub>25</sub> and marine phytoplankton biomarkers, with PIP<sub>25</sub> values indicating the presence of seasonal sea ice (Fig. 3). Although the emergence of seasonal sea ice aligns with the warmer climate of this period (Shakun et al., 2012), large-scale Arctic sea ice records suggest that the elevated temperatures were not drivers of the breakup of permanent sea ice. This is evident from the observations that sea ice in regions like the Beaufort Sea and  
300 Laptev Sea was reduced during the cold deglaciation and expanded during the warm late Holocene (Fig. 4; Wu et al., 2020; Fahl and Stein, 2012; Hörner et al., 2016). Instead, the transition was likely driven by orbital forcing, as summer insolation at 70°N reached its maximum during this time (Laskar et al., 2004; Stranne et al., 2014). Comparisons with sea ice records from the nearby Laptev Sea reveal contrasting patterns during the early Holocene: while sea ice over the Southern Lomonosov Ridge transitioned from permanent to seasonal sea ice, sea ice coverage in the Laptev Sea increased (Fig. 4; Hörner et al.,  
305 2016; Lin et al., 2024). This suggests that the orbital forcing, rather than warm Atlantic Water, became the dominant factor influencing sea ice dynamics during this period.

During the PB/EH, there was a substantial increase in terrestrial biomarkers of campesterol and  $\beta$ -sitosterol, even surpassing levels observed during the DO-3 (Fig. 3). Source apportionment and elevated pre-depositional ages (7500-15000 years) suggest  
310 a significant input of ICD-OC (Fig. 5), which is likely linked to coastal erosion driven by sea-level rise during the MWP-1B (Lambeck et al., 2014; Martens et al., 2020). This finding is consistent with massive permafrost carbon remobilization recorded in the Laptev Sea, Chukchi Sea, Beaufort Sea, Okhotsk Sea, Bering Sea, and North Pacific (Tesi et al., 2016; Martens et al., 2019; Wu et al., 2022; Winterfeld et al., 2018; Meyer et al., 2019; Lin et al., 2024). However, a role of concurrent sea ice reduction cannot be excluded. Seasonal sea ice can promote wave-induced coastal erosion of ICD by increasing fetch distance  
315 under frequent open water conditions (Barnhart et al., 2014). Additionally, open water conditions can further elevate heat and moisture transport, potentially leading to deeper thaws of permafrost (Vaks et al., 2020). Therefore, it is plausible that sea-level rise and sea ice reduction acted synergistically to increase destabilization of coastal permafrost, although their relative contributions remain unclear.

#### **4.5 Gradual buildup of extended sea ice during the Late-Mid Holocene**

320 Following the rapid decline in sea ice cover during the PB/EH transition, the Mid-Late Holocene is characterized by relatively stable environmental conditions. Starting around 7.5 kyr B.P., marine and sea ice algae productivity gradually diminished, indicating a buildup of a more extended sea ice cover (Fig.3). The trend of expanding Arctic sea ice towards the Late Holocene, as observed in our record, is consistent with findings from the Beaufort Sea, Kara Sea, Chukchi Sea, Laptev Sea, and East Siberian Sea (Fig. 5; Fahl & Stein, 2012; Hörner et al., 2016; Stein et al., 2017; Hörner et al., 2018; Wu et al., 2020; Dong et al., 2022). The primary driver of this sea ice expansion during the Late Holocene is hypothesized to be the reduction in summer  
325 solar insolation, which resulted in decreased heat available for melting sea ice (Dong et al., 2022).



Coinciding with the expanding sea ice cover, the input of campesterol and  $\beta$ -sitosterol gradually decreased throughout the Holocene, implying a decline in terrOC contribution in tandem with reduced marine productivity (Fig. 3 & 4). This trend of minimal terrOC input and OC deposition is consistently observed in the Laptev Sea and East Siberian Sea (Tesi et al., 2016; Keskitalo et al., 2017; Martens et al., 2020). Although the OC input remained low during the Holocene, the relative influence of marine sources became more important towards the Late Holocene (Fahl & Stein 2012; Martens et al., 2020). The terrOC remobilization of permafrost pools reduced, likely due to the relatively stable climatic conditions that did not trigger significant OC remobilization, as had occurred during earlier periods of rapid temperature rise.

## 335 5 Conclusions

This study reconstructed sea ice history over the past 27 kyrs at the Southern Lomonosov Ridge using sea ice biomarkers IP<sub>25</sub> and open-water algae biomarkers brassicasterol and dinosterol, providing a comprehensive record that spans the late DO-3 and LGM through the deglaciation period. This work offers new insights into past sea ice variability and its controlling mechanisms. With emerging studies suggesting that sea ice can indirectly influence permafrost thaw and mobilization by modulating wave activity, heat, and moisture transport, we integrated our sea ice reconstruction with previously detailed investigations of permafrost carbon remobilization from the same core. The combined approach sheds light on the role of sea ice in influencing permafrost thaw under climate change. The key findings of this study are as follows.

1. The sea ice over the Lomonosov Ridge exhibited seasonal variability following the DO-3 interstadial, followed by the establishment of permanent sea ice persisting until 11 kyr BP. The breakup of this permanent sea ice occurred during the early Holocene, leading to a period of low sea ice concentrations, which then gradually increased through the mid-late Holocene.
2. Compared to sea ice records from the nearby Laptev Sea, the warm Atlantic water inflow likely played a primary role in the contrasting sea ice conditions between these two regions during the deglaciation: while the Lomonosov Ridge experienced permanent sea ice, the Western Laptev Sea was characterized by seasonal/ice-free conditions. The breakup of permanent sea ice during the early Holocene, followed by a subsequent expansion, is consistent with records from other parts of the Arctic Ocean, suggesting a predominant influence of orbital forcing during this period.
3. Permafrost carbon remobilization occurred after DO-3, during B/A, and PB/EH interstadials. The reduction in sea ice after DO-3 and PB/EH likely contributed to permafrost destabilization by modulating wave activity and heat/moisture transport, which further enhanced coastal erosion and inland permafrost thaw. In contrast, the moderate carbon remobilization observed during the B/A, compared to DO-3 and PB/EH, may indicate that permanent sea ice to some degree have protected Arctic coastlines. Therefore, the magnitude of permafrost-carbon remobilization could be attenuated by permanent sea ice.



### **Data availability**

360 The supplementary dataset can be accessed on the Bolin Centre Database (link to be published).

### **Author contributions**

The study was conceptualized by Ö.G and J.W. Sediment sampling was conducted by M.R. Laboratory work, methodology and creation of the first manuscript draft was made by A.E under supervision of J.W and Ö.G. All authors have contributed to data interpretation and writing of the manuscript.

### **365 Competing interests**

The authors declare no conflicts of interest.

### **Acknowledgments**

We thank the crew onboard the Swedish icebreaker *Oden* for the sampling of 31-PC. We also thank Dr. Francesco Muschitiello for the work on the age-model of 31-PC (Muschitiello et al., 2020), and Dr. Jannik Martens for conducting previous carbon  
370 geochemistry analyses (Martens et al., 2020). We further thank Dr. Wen Zhang for assisting with the analytical protocol, and Professor Simon Belt for providing reference sediments to enable quantifications of IP<sub>25</sub>.

### **Financial support**

The SWERUS-C3 program was supported by the Knut and Alice Wallenberg Foundation (KAW contract 2011.0027 to Ö.G) and the Swedish Research Council (VR contract 621-2013-5297 to Ö.G). This study was also supported by the European  
375 Research Council (ERC AdG CC-TOP 695331 to Ö.G.) and the VR Distinguished Professorship Program (contract 621-2017-01601 to Ö.G.).



## References

- 380 Barnhart, K.R., Overeem, I., and Anderson, R.S.: The effect of changing sea ice on the physical vulnerability of Arctic coasts, *The Cryosphere*, 8, 1777-1779, <https://doi.org/10.5194/tc-8-1777-2014>, 2014.
- Belt, S. T., Massé, G., Rowland, S. J., Poulin, M., Michel, C., and LeBlanc, B.: A novel chemical fossil of palaeo sea ice: IP<sub>25</sub>, *Org. Geochem.*, 38, 16–27, <https://doi.org/10.1016/j.orggeochem.2006.09.013>, 2007.
- 385 Belt, S.T., Brown, T.A., Navarro Rodriguez, A., Cabedo Sanz, P., Tonkin, A., and Ingle, R.: A reproducible method for the extraction, identification, and quantification of the Arctic sea ice proxy IP<sub>25</sub> from marine sediments, *Analytical methods*, 4, 705-713. <https://doi.org/10.1039/C2AY05728J>, 2012.
- Belt, S.: Source-specific biomarkers as proxies for Arctic and Antarctic sea ice, *Organic Geochemistry*, 125, 277-298, <https://doi.org/10.1016/j.orggeochem.2018.10.002>, 2018.
- 390 Bradley, R.S., and England, J.H.: The Younger Dryas and the Sea of Ancient Ice, *Quaternary Research*, 70, 1-10, <https://doi.org/10.1016/j.yqres.2008.03.002>, 2008.
- 395 Bröder, L., Tesi, T., Andersson, A., Semiletov, I., and Gustafsson, Ö.: Bounding cross-shelf transport time and degradation in Siberian-Arctic land-ocean carbon transfer, *Nat. Comm*, 9, 806, <https://doi.org/10.1038/s41467-018-03192-1>, 2018.
- Cao, M., Hefter, J., Tiedemann, R., Lembke-Jene, L., Meyer, V. D., and Mollenhauer, G.: Deglacial records of terrigenous organic matter accumulation off the Yukon and Amur rivers based on lignin phenols and long-chain *n*-alkanes, *Clim. Past*, 19, <https://doi.org/10.5194/cp-19-159-2023>, 2023.
- 400 Dansgaard, W., Johnsen, S.J., Clausen, H.B., Dahl-Jensen, D., Gundestrup, N.S., Hammer, C.U., Hvidberg, C.S., Steffensen, J.P., Sveinbjörnsdóttir, A.E., Jouzel, J., and Bond, G.: Evidence for general instability of past climate from a 250-kyr ice-core record, *Nature*, 364, 218-220, <https://doi.org/10.1038/364218a0>, 1993.
- 405 Dong, J., Shi, X., Gong, X., Astakhov, A.S., Hu, L., Liu, X., Yang, G., Wang, Y., Vasilenko, Y., Qiao, S., Bosin, A., and Lohmann, G.: Enhanced Arctic sea ice melting controlled by larger heat discharge of mid-Holocene rivers, *Nature Communications*, 13, 5368, <https://doi.org/10.1038/s41467-022-33106-1>, 2022.



- 410 Duan, L., Cao, L., and Caldeira, K.: Estimating Contributions of Sea Ice and Land Snow to Climate Feedback, *Atmospheres*, 124(1), 199-208, <https://doi.org/10.1029/2018JD029093>, 2019.
- Fahl, K., and Stein, R.: Biomarkers as organic-carbon-source and environmental indicators in the Late Quaternary Arctic Ocean: problems and perspectives, *Marine Chemistry*, 63, 293-309, [https://doi.org/10.1016/S0304-4203\(98\)00068-1](https://doi.org/10.1016/S0304-4203(98)00068-1), 2012.
- 415 Gustafsson, Ö., van Dongen, B. E., Vonk, J. E., Dudarev, O. V., and Semiletov, I. P.: Widespread release of old carbon across the Siberian Arctic echoed by its large rivers, *Biogeosciences*, 8, 1737–1743, <https://doi.org/10.5194/bg-8-1737-2011>, 2011.
- Hörner, T., Stein, R., Fahl, K., and Birgel, D.: Post-glacial variability of sea ice cover, river run-off and biological production in the western Laptev Sea (Arctic Ocean) – A highresolution biomarker study, *Quaternary Science Reviews*, 143, 133-149, <https://doi.org/10.1016/j.quascirev.2016.04.011>, 2016.
- 420 Hörner, T., Stein, R., and Fahl, K.: Paleo-sea ice distribution and polynya variability on the Kara Sea shelf during the last 12 ka, 4, 11-16, <https://doi.org/10.1007/s41063-018-0040-4>, 2018.
- 425 Jakobsson, M., Mayer, L.A., Bringensparr, C. et al.: The International Bathymetric Chart of the Arctic Ocean Version 4.2. *Sci Data* 7, 176, <https://doi.org/10.1038/s41597-020-0520-9>, 2022.
- Jensen, M.G., Nummelin, A., Nielsen, S.B., Sadatzki, H., Sessford, E., Risebrobakken, B., Andersson, C., Voelker, A., Roberts, W.H.G., Pedro, J., and Born, A.: A spatiotemporal reconstruction of sea-surface temperatures in the North Atlantic during Dansgaard–Oeschger events 5–8, *Clim. Past*, 14, 901–922, <https://doi.org/10.5194/cp-14-901-2018>, 2018.
- 430 Karlsson, E., Gelting, J., Tesi, T., van Dongen, B., Andersson, A., Semiletov, I., Charkin, A., Dudarev, O., and Gustafsson, Ö.: Different sources and degradation state of dissolved, particulate, and sedimentary organic matter along the Eurasian Arctic coastal margin, *Global Biogeochem. Cycles*, 30, 898-919, <https://doi.org/10.1002/2015GB005307>, 2016.
- 435 Keskitalo, K., Tesi, T., Bröder, L., Andersson, A., Pearce, C., Sköld, M., Semiletov, I. P., Dudarev, O. V., and Gustafsson, Ö.: Sources and characteristics of terrestrial carbon in Holocene-scale sediments of the East Siberian Sea, *Clim. Past*, 13, 1213–1226, <https://doi.org/10.5194/cp-13-1213-2017>, 2017.
- 440 Kremer, A., Stein, R., Fahl, K., Bauch, H., Mackensen, A., and Niessen, F.: A 190-ka biomarker record revealing interactions between sea ice, Atlantic Water inflow and ice sheet activity in eastern Fram Strait, *Arktos*, 4, 11-17, <https://doi.org/10.1007/s41063-018-0052-0>, 2018.



Köhler, P., Knorr, G., and Bard, E.: Permafrost thawing as a possible source of abrupt carbon release at the onset of the  
445 Bølling/Allerød, *Nature Communications*, 5, 5520, <https://doi.org/10.1038/ncomms6520>, 2014.

Lambeck, K., Rouby, H., Purcell, A., Sun, Y., and Sambridge, M.: Sea level and global ice volumes from the Last Glacial  
Maximum to the Holocene, *P. Natl. Acad. Sci. USA*, 111(43), 15296-15303, <https://doi.org/10.1073/pnas.1411762111>, 2014.

450 Laskar, J., Robutel, P., Joutel, F., Gastineau, M., Correia, A.C.M., and Levrard, B.: A long-term numerical solution for the  
insolation quantities of the Earth *Astronomy & Astrophysics*, 428(1), 261-285, <https://doi.org/10.1051/0004-6361:20041335>,  
2004.

Lin, T.-W., Tesi, T., Hefter, J., Grotheer, H., Wollenburg, J., Adolphi, F., Bauch, H. A., Nogarotto, A., Müller, J., and  
455 Mollenhauer, G.: Environmental controls of rapid terrestrial organic matter mobilization to the western Laptev Sea since the  
Last Deglaciation, *Clim. Past*, 21, 753–772, <https://doi.org/10.5194/cp-21-753-2025>, 2025.

Martens, J., Wild, B., Muschitiello, F., O'Regan, M., Jakobsson, M., Semiletov, I., Dudarev, O.V., and Gustafsson, Ö.:  
Remobilization of dormant carbon from Siberian-Arctic permafrost during three past warming events, *Science Advances*, 6,  
460 eabb6546, <https://doi.org/10.1126/sciadv.abb6546>, 2020.

Martens, J., Romankevich, E., Semiletov, I., Wild, B., van Dongen, B., Vonk, J., Tesi, T., Shakhova, N., Dudarev, O. V.,  
Kosmach, D., Vetrov, A., Lobkovsky, L., Belyaev, N., Macdonald, R. W., Pieńkowski, A. J., Eglinton, T. I., Haghypour, N.,  
Dahle, S., Carroll, M. L., Åström, E. K. L., Grebmeier, J. M., Cooper, L. W., Possnert, G., and Gustafsson, Ö.: CASCADE –  
465 The Circum-Arctic Sediment CARbon DatabasE, *Earth Syst. Sci. Data*, 13, 2561–2572, [https://doi.org/10.5194/essd-13-2561-](https://doi.org/10.5194/essd-13-2561-2021)  
2021, 2021.

Martens, J., Wild, B., Semiletov, I., Dudarev, O.V., and Gustafsson, Ö.: Circum-Arctic release of terrestrial carbon varies  
between regions and sources, *Nature Communications*, 13, 5858, <https://doi.org/10.1038/s41467-022-33541-0>, 2022.

470

Matsubara, F., Wild, B., Martens, J., Andersson, A., Wennström, R., Bröder, L., Dudarev, O.V., Semiletov, I., and Gustafsson,  
Ö.: Molecular-Multiproxy Assessment of Land-Derived Organic Matter Degradation Over Extensive Scales of the East  
Siberian Arctic Shelf Seas, *Global Biogeochemical Cycles*, 36, e2022GB007428, <https://doi.org/10.1029/2022GB007428>,  
2022.

475



- Meyer, V., Hefter, J., Köhler, P., Tiedemann, R., Gersonde, R., Wacker, L., and Mollenhauer, G.: Permafrost-carbon mobilization in Beringia caused by deglacial meltwater runoff, sea-level rise and warming, 14(8), 085003, *Environ. Res. Lett.* <https://doi.org/10.1088/1748-9326/ab2653>, 2019.
- 480 Müller, J., Wagner, A., Fahl, K., Stein, R., Prange, M., and Lohmann, G.: Towards quantitative sea ice reconstructions in the northern North Atlantic: A combined biomarker and numerical modelling approach, *Earth and Planetary Science Letters*, 306, 137-148, <https://doi.org/10.1016/j.epsl.2011.04.011>, 2011.
- Muschitiello, F., O'Regan, M., Martens, J., West, G., Gustafsson, Ö., and Jakobsson, M.: A new 30 000-year chronology for rapidly deposited sediments on the Lomonosov Ridge using bulk radiocarbon dating and probabilistic stratigraphic alignment, *Geochronology*, 2, 81–91, <https://doi.org/10.5194/gchron-2-81-2020>, 2020.
- 485 Nicolas, A., Hefter, J., Grotheer, H., Tesi, T., Stein, R., Nogarotto, A., Alves, E.Q., Mollenhauer, G.: Delivery of aged terrestrial organic matter to the Laptev Sea during the last deglaciation, *Clim. Past*, 21, 2579-2599, [https://doi.org/10.5194/cp-](https://doi.org/10.5194/cp-21-2579-2025)
- 490 21-2579-2025, 2025.
- Nielsen, D.M., Dobrynin, M., Baehr, J., Razumov, S., and Grigoriev, M.: Coastal Erosion Variability at the Southern Laptev Sea Linked to Winter Sea Ice and the Arctic Oscillation, *Geophysical Research Letters*, 47, e2019GL086876, <https://doi.org/10.1029/2019GL086876>, 2020.
- 495 Nielsen, D.M., Chegini, F., Maerz, J., Brune, S., Mathis, M., Dobrynin, M., Baehr, J., Brovkin, V., and Ilyina, T.: Reduced Arctic Ocean CO<sub>2</sub> uptake due to coastal permafrost erosion, *Nature Climate Change*, <https://doi.org/10.1038/s41558-024-02074-3>, 2024.
- 500 Overduin, P.P., Schneider von Deimling, T., Meisner, F., Grigoriev, M.N., Ruppel, C., Vasilev, A., Lantuit, H., Juhls, H., Westermann, S.: Submarine Permafrost Map in the Arctic Modeled Using 1-D Transient Heat Flux (SuPerMAP), *JGR Oceans*, 124, 6, 3487-3507, <https://doi.org/10.1029/2018JC014675>, 2019.
- Overeem, I., Anderson, R.S., Wobus, C.W., Clow, G.D., Urban, F.E., and Matell, N.: Sea ice loss enhances wave action at the Arctic coast, *Geophysical Research Letters*, 38, L17503, <http://dx.doi.org/10.1029/2011GL048681>, 2011.
- 505 Reimer, P.J., Austin, W.E.N., Bard, E., et al.: The IntCal20 Northern Hemisphere Radiocarbon Age Calibration Curve (0-55 kBP), *Radiocarbon*, 62(4): 725-757, <https://doi.org/10.1017/RDC.2020.41>, 2020.



510 Semiletov, I., Dudarev, O., Luchin, V., Charkin, A., Shin, K.H., and Tanaka, N.: The East Siberian Sea as a transition zone between Pacific-derived waters and Arctic shelf waters, *Geophysical Research Letters*, 32, L10614, <https://doi.org/10.1029/2005GL022490>, 2005.

Sévellec, F., Fedorov, A.V., and Liu, W.: Arctic sea-ice decline weakens the Atlantic Meridional Overturning Circulation, *Nature Climate Change*, 7, 604-610, <https://doi.org/10.1038/nclimate3353>, 2017.

Shakun, J.D., Clark, P.U., He, F., Marcot, S.A., Mix, A.C., Zhengyu, L., Otto-Bliesner, B., Schmittner, A., and Bard, E.: Global warming preceded by increasing carbon dioxide concentrations during the last deglaciation, *Nature*, 484, 49-54, <https://doi.org/10.1038/nature10915>, 2012.

520

Schefuß, E., Eglinton, T., Spencer-Jones, C. et al.: Hydrologic control of carbon cycling and aged carbon discharge in the Congo River basin, *Nature, Geosci*, 9, 687-690, <https://doi.org/10.1038/ngeo2778>, 2016.

525 Solomon, A.: Impact of latent heat release on polar climate, 33(7), *Geophysical Research Letters*, 33 (7), <https://doi.org/10.1029/2005GL025607>, 2006.

Stein, R., and Fahl, K.: A first southern Lomonosov Ridge (Arctic Ocean) 60 ka IP25 sea-ice record, *Polarforschung*, 82, 83-86, <http://hdl.handle.net/10013/epic.40434.d001>, 2012.

530

Stein, R., Fahl, K., Schade, I., Manerung, A., Wassmuth, S., Niessen, F., and Nam, S.: Holocene variability in sea ice cover, primary production, and Pacific-Water inflow and climate change in the Chukchi and East Siberian Seas (Arctic Ocean), 32, 362-379, <https://doi.org/10.1002/jqs.2929>, 2017.

535 Stranne, C., Jakobsson, M., and Björk, G.: Arctic Ocean perennial sea ice breakdown during the Early Holocene Insolation Maximum. *Quaternary Science Reviews*, 92, 123-132, <https://doi.org/10.1016/j.quascirev.2013.10.022>, 2014.

Strauss, J., Schirrmesiter, L., Grosse, G., Fortier, D., Hugelius, G., Knoblach, C., Romanovsky, V., Schädel, C., Schneider von Deimling, T., Schuur, E.A.G., Shmelev, D., Ulrich, M., and Veremeeva, A.: Deep Yedoma permafrost: A synthesis of  
540 depositional characteristics and carbon vulnerability, *Earth Science Reviews*, 172, 75-86, <https://doi.org/10.1016/j.earscirev.2017.07.007>, 2017.



Strauss, J., Laboor, S., Schirrmeister, L., Fedorov, A.N., Fortier, D., Froese, D.G., Fuchs, M., Günther, F., Grigoriev, M.N., Harden, J.W., Hugelius, G., Jongejans, L.L., Kanevskiy, M.Z., Kholodov, A.L., Kunitsky, V., Kraev, G., Lozhkin, A. V.,  
545 Rivkina, E., Shur, Y., Siegert, C., Spektor, V., Streletskaia, I., Ulrich, M., Vartanyan, S.L., Veremeeva, A., Walter A. K.,  
Wetterich, S., Zimov, N.S., and Grosse, G.: Database of Ice-Rich Yedoma Permafrost Version 2 (IRYP v2), PANGAEA,  
<https://doi.org/10.1594/PANGAEA.940078>, 2022.

Taylor, P.C., Cai, M., Hu, A., Meehl, J., Washington, W., and Zhang, G.J.: A Decomposition of Feedback Contributions to  
550 Polar Warming Amplification, *Journal of Climate*, 26 (18), 7023-7043, <https://doi.org/10.1175/JCLI-D-12-00696.1>, 2013.

Tesi, T., Muschitiello, F., Smittenberg, R.H., Jakobsson, M., Vonk, J.E., Hill, P., Andersson, A., Kirchner, N., Noormets, R.,  
Dudarev, O., Semiletov, I., and Gustafsson, Ö.: Massive remobilization of permafrost carbon during post-glacial warming,  
*Nature Communications*, 7, 13653, <https://doi.org/10.1038/ncomms13653>, 2016.

555

Vaks, A., Mason, A.J., Breitenbach, S.F.M., Kononov, A.M., Osinzev, A.V., Rosensaft, M., Morshevsky, A., Gutareva, O.S.,  
and Henderson, G.M.: Palaeoclimate evidence of vulnerable permafrost during times of low sea ice, *Nature*, 577, 221-225,  
<https://doi.org/10.1038/s41586-019-1880-1>, 2020.

560 Vonk, J.E., Sánchez-García, L., van Dongen, B.E., Alling, V., Kosmach, D., Charkin, A., Semiletov, I.P., Dudarev, O.V.,  
Shakhova, N., Roos, P., Eglinton, T.I., Andersson, A., and Gustafsson, Ö.: Activation of old carbon by erosion of coastal and  
subsea permafrost in Arctic Siberia, *Nature*, 489, 137-140, <https://doi.org/10.1038/nature11392>, 2012.

Vonk, J.E., Fritz, M., Speetjens, N.J., Babin, M., Bartsch, A., Basso, L.S., Bröder, L., Göckede, M., Gustafsson, Ö., Hugelius,  
565 G., Irrgang, A.M., Juhls, B., Kuhn, M. A., Lantuit, H., Manizza, M., Martens, J., O'Regan, M., Suslova, A., Tank, S.E., Terhaar,  
J., and Zolkos, S.: The land-ocean Arctic carbon cycle, *Nat Rev Earth Environ*, 6, 86-105, <https://doi.org/10.1038/s43017-024-00627-w>, 2025.

Wild, B., Andersson, A., Bröder, L., Vonk, J., Hugelius, G., McClelland, J.W., Song, W., Raymond, P.A., and Gustafsson, Ö.:  
570 Rivers across the Siberian Arctic unearth the patterns of carbon release from thawing permafrost, *PNAS*, 116, 10280-10285,  
<https://doi.org/10.1073/pnas.1811797116>, 2019.

Winterfeld, M., Mollenhauer, G., Dumann, W., Köhler, P., Lembke-Jene, L., Hefter, J., McIntyre, C., Wacker, L., Kokfelt,  
U., and Tiedemann, R.: Deglacial mobilization of pre-aged terrestrial carbon from degrading permafrost, *Nature*  
575 *Communications*, 9, 3666, <https://doi.org/10.1038/s41467-018-06080-w>, 2018.



Wu, J., Stein, R., Fahl, K., Syring, N., Seung-II, N., Hefter, J., Mollenhauer, G., and Gilbert, W.: Deglacial to Holocene variability in surface water characteristics and major floods in the Beaufort Sea, *Communications Earth and Environment*, 1, 27, <https://doi.org/10.1038/s43247-020-00028-z>, 2020.

580

Wu, J., Mollenhauer, G., Stein, R., Köhler, P., Hefter, J., Fahl, K., Grotheer, H., Wei, B., and Nam, S.: Deglacial release of petrogenic and permafrost carbon from the Canadian Arctic impacting the carbon cycle, *Nat. Commun*, 13, 7172, <https://doi.org/10.1038/s41467-022-34725-4>, 2022.

585 Wu, J., Matsubara, F., Mollenhauer, G., Stein, R., Wei, B., Fahl, K., Xiao, X., and Gustafsson, Ö.: Geospatial patterns in terrestrial organic matter reactivity across four shelf seas spanning the Eurasian Arctic, *Sci Adv*, 11, eadt6806, <https://doi.org/10.1126/sciadv.adt6806>, 2025.

Xiao, X., Fahl, K., and Stein, R.: Biomarker distributions in surface sediments from the Kara and Laptev seas (Arctic Ocean): indicators for organic-carbon sources and sea-ice coverage, *Quaternary Science Reviews*, 79, 40-52, <https://doi.org/10.1016/j.quascirev.2012.11.028>, 2013.

590 Xiao, X., Stein, R., and Fahl, K.: MIS 3 to MIS 1 temporal and LGM spatial variability in Arctic Ocean sea ice cover: Reconstruction from biomarkers, *Paleoceanography and Paleoclimatology*, 30, 969-983, <https://doi.org/10.1002/2015PA002814>, 2015.

595